Laser-Induced Fluorescence of Xe I and Xe II in Ambipolar Plasma Flow

Panagiotis Svarnas, *Senior Member, IEEE*, Ivan Romadanov, Ahmed Diallo, and Yevgeny Raitses

***Abstract*— Laser-induced fluorescence diagnostic technique is applied here to probe xenon neutrals and single-charged ions in an ambipolar plasma source. A single tunable diode laser is employed for pumping both following transitions: $6s\ ^2[1/2]^0_1$–$6p\ ^2[3/2]^0_1$ (centered at 834.68 nm; air) and $5d[4]_{7/2}$–$6p[3]_{5/2}$ (centered at 834.72 nm; air), for Xe I and Xe II detection, respectively. The corresponding decay states are $6s[3/2]^0_1$ and $6s[2]_{3/2}$ leading to fluorescence signal at 473.415 and 541.915 nm, respectively. A detailed description of the experimental setup along with time-averaged fluorescence signals are presented, demonstrating the possible application of the above adjacent pumping wavelengths in xenon ambipolar plasmas for probing both ions and neutrals under various operating conditions. A comprehensible discussion to what extent the registered laser-induced fluorescence signals mirror velocity distribution functions is realized, following hyperfine splitting and isotopic shift analysis.**

***Index Terms*— Ambipolar plasmas, cylindrical hall thrusters (CHTs), laser-induced fluorescence, xenon gas.**

I. Introduction

A. Ambipolar Plasmas and the Need for Studying Both Neutrals and Ions

AMBIPOLAR plasma sources are used for plasma thrusters [1], [2], plasma cathodes [3], [4], plasma processing [5], [6], and basic plasma studies [7], [8]. For plasma propulsion, ambipolar plasma sources with simplified design without magnetic field offer the feasibility of implementation of miniaturized dc and RF low-power (<100 W) plasma thrusters for small satellites. The common principle of all ambipolar plasma sources is that they generate weakly collisional plasma in a channel by either dc or RF discharge and produce nonequilibrium plasma flow through the opening of the channel. A detailed knowledge of velocity distribution functions (VDFs) for both ions and neutrals is critically important for characterization of the plasma flow and understanding of plasma kinetic processes.

Manuscript received November 3, 2016; revised June 2, 2018; accepted July 11, 2018. This work was supported in part by the U.S. Department of Energy under DOE Contract DE-AC02-09CH11466 and in part by the Air Force Office of Scientific Research. The review of this paper was arranged by Senior Editor S. J. Gitomer. *(Corresponding author: Panagiotis Svarnas.)*

P. Svarnas is with the High Voltage Laboratory, Electrical and Computer Engineering Department, University of Patras, 26504 Rion-Patras, Greece (e-mail: svarnas@ece.upatras.gr).

I. Romadanov is with the Department of Physics and Engineering Physics, University of Saskatchewan, Saskatoon SK S7N 5E2, Canada.

A. Diallo and Y. Raitses are with the Princeton Plasma Physics Laboratory, Princeton, NJ 08540 USA.

Color versions of one or more of the figures in this paper are available online at http://ieeexplore.ieee.org.

Digital Object Identifier 10.1109/TPS.2018.2857508

Regarding ionized species, the velocity distribution is essential because it determines the stability of the plasma medium, e.g., in cases where strong anisotropy is induced by the application of a magnetic field which gives rise to several effects connected to the cyclotronic motion of the particles [9]. Besides, it has been mentioned in earlier works that the electric field topology can cause back flow of ions, affecting the lifetime of a thruster due to erosion processes. Beal *et al.* [10] studied the effects of clustering multiple Hall thrusters on plasma plume properties and it was shown that in the region between the thrusters, the plasma potential increases as a function of downstream distance and may result in reflection of some low-energy ions back toward the cluster. The features of such backscattering ions can be detected on the ion velocity distributions where they appear as a negative-velocity component. Furthermore, ion VDF is a key in the study of the divergence of the ion beam in thrusters. A large divergence leads to reduction in the thrust, and the magnetic field optimization is critical for divergence reduction [11]. The exploitation of additional effects, like highly supersonic ion beams generated by current-free double layers, can profit of ion VDF recording in ambipolar plasmas [12]. Parameters such as the spatially and time-dependent ion VDFs can directly impact the performance of plasma systems and yield insight into ionization mechanisms, electric potential formation and acceleration regions [13].

In the case of neutrals, neutral dynamics could affect the shaping of ion VDFs, and thrust mechanisms could be reflected on neutral and ion VDFs. For instance, it has been reported that neutral depletion may occur in significant portions of a thruster plume and that a neutral ionization mechanism is active in the plasma flow traveling away from the exit plane. Electron impact ionization and/or ion–neutral collisions are the likely causes of the neutral depletion. Cold background gas diffuses into the ion beam over its length, acting to partially replenish what is lost. Conversion of fast ions to slower ions via ion–neutral collisions and subsequent acceleration in the local electric field may increase total plume 'momentum and registered thrust [14]. It has also been reported that creation of fast neutrals at walls has a direct impact on the Hall thruster discharge properties [15]. In addition, it has been shown that neutral flow mechanisms can play a very important role in controlling the location and properties of the plasma in a Hall thruster [16].

The focus of this paper is thus on the validation of a quite simple experimental setup which leads to both ionic and atomic VDF determination at different operating conditions.

B. LIF Fundamentals and Line-Shaped Distortions

The setup refers to laser-induced fluorescence (LIF) technique with nonresonant signal detection. LIF presents a nonintrusive, species-specific, spatially resolved approach for obtaining VDFs based on the Doppler shift of given species. Briefly [17]–[19]: LIF operates on the principle that when a particle in the lower energy state absorbs a photon and rises up to higher energy state, it will deexcite and emit another photon. Excited particles will decay by collision, spontaneous emission, or stimulated emission. Particles that spontaneously emit photons at the same energy as the absorbed photons are said to undergo resonant emission. Particles that emit photons at energies different from that of the absorbed photons are said to undergo nonresonant emission. This spontaneous emission, called fluorescence, radiates isotropically away from the particle. To obtain the particle VDF via LIF, one takes advantage of the Doppler shift. For a particle traveling at nonrelativistic speed, the shift in the absorption frequency is proportional to the particle velocity component in the direction that the photon travels. This is described mathematically by the following equation [17]:

$$\frac{\Delta \upsilon}{\upsilon_0} = -\frac{\mathbf{v}}{c}\frac{\mathbf{k}}{|\mathbf{k}|} \tag{1}$$

where υ_0 stands for the photon frequency, $\Delta\upsilon$ stands for the shift in photon frequency from the perspective of the particle, $\mathbf{v}$ is the particle velocity, c is the speed of light, and $\mathbf{k}$ is the photon wave vector. By varying the frequency of the incident photons and comparing the intensity of the collected fluorescence, one can obtain the particle VDF along the incident photon wave vector. Thus, velocity component distinction is also possible. Even though relative experimental setups are rather complex and delicate, especially when dye lasers are involved, the advanced specifications and the robustness of currently available diode laser sources (in terms of spectral linewidth, frequency and intensity noises, power, and possibility of stable and reliable optical fiber coupling) make it possible to engineer robust and user-friendly devices for both ion and neutral dynamic studies [20].

However, different physical mechanisms determine eventually the recorded line shape, i.e., the raw LIF spectrum, making thus the line shape to deviate from the particle VDF. Weak magnetic field effect (Zeeman splitting), electric field effect (Stark splitting), isotopic shifts (ISs), hyperfine structures (HFS), and natural (lifetime) broadening, which is due to the Heisenberg uncertainty principle, of the considered pumped transitions are potential distortion sources. For instance, many effects like charge exchange and partial ion acceleration show up as tails in ion VDFs. The accuracy with which the magnitude of these low-lying populations can be calculated is highly dependent on properly deconvolving out IS and HFS [17]. The potential involvement of the above-mentioned effects in the results of this paper is discussed in Section III.

It is reminded that when the absorbing species velocity distribution is Maxwellian, the Doppler broadening results in a Gaussian line shape. Collisional interactions between the absorbers and other species in the plasma give rise to spectral line shapes that are Lorentzian. If both Doppler and collisional broadening are important and independent, the resulting line shape is a convolution of the Gaussian and Lorentzian line shape into a Voigt line shape [19]. Natural broadening also broadens an absorption line into a Lorentzian function [21].

C. Representative Bibliography on LIF of Xe I and Xe II

Plasma propulsion, especially Hall thrusters, ion thrusters, and RF plasma thrusters, benefited a lot from the development of LIF techniques for measurements of mainly ion VDFs inside these thrusters and in the thruster plume [22], [23]. Xenon gas is considered as the most typical propellant due to its favorable ionization properties (lowest ionization potential and largest cross section for ionization among other gas propellants) and high atomic mass which are needed for thrust production. Therefore, a majority of LIF studies in the field of plasma propulsion are focused on xenon plasma flow. Below, a literature indicative review of previous relevant works is briefly presented. First, works on Xe II are given in chronological order, and then works on Xe I and "Xe I and Xe II" are cited again in chronological order.

Manzella [24] interrogated the exhaust of a 1.5-kW stationary plasma thruster by LIF, using the $5d\ ^4[F]_{5/2}$–$6p\ ^4[D]_{5/2}$ Xe II transition (pumping at 834.7 nm). The laser employed was a commercially available continuous wave (CW), single-mode, GaAlAs semiconductor laser with a nominal center wavelength of 845 nm and a linewidth of approximately 15 MHz. Gascon *et al.* [25] measured the ionized propellant velocities at 834.7 nm in the Stanford Linear Hall thruster, by employing a tunable diode laser similar to the one used in our work. In Gascon's [25] work, the absorption of the 834.687-nm Xe I transition was mentioned as well, but just as a stationary reference for measurement of the Doppler-shifted ionic transition. Neutrals were thus excited in a low-pressure Xe hollow cathode lamp, and their study in the thruster was not the object of that work. Smith *et al.* [26] presented results from the optogalvanic and LIF measurements of the nuclear-spin and isotopic structure of the $5d\ ^2[F]_{7/2}6p\ ^2[D]^0_{5/2}$ Xe II transition at 834.7 nm. As for their LIF setup, the primary laser was a tapered-amplifier diode laser and their secondary system a dye laser. Huang *et al.* [17] presented and validated a method for extracting velocity distribution functions from diode LIF measurements in an ion source plume, using the $5d[4]_{7/2}$–$6p[3]^0_{5/2}$ transition of Xe II (834.7 nm) without the need to know the hyperfine constants. Spektor *et al.* [27] excited the $5d\ ^4[F]_{7/2}$–$6p\ ^4[D]_{5/2}$ transition of Xe II with a tunable diode laser and recorded time-averaged ion velocity profiles in a cylindrical Hall thruster (CHT) plume. Biloiu and Scime [28] investigated ion VDFs by LIF in Ar–Xe and Ar–He expanding helicon plasmas as a function of gas composition. A continuous-wave Ar ion-pumped dye laser that pumps transitions for both Ar^+ and Xe^+ was employed. For Xe^+, the transition $(5d\ ^4D_{7/2})$–$(6p\ ^4P_{5/2})$ at 605.278 nm was probed. Vaudolon *et al.* [29] probed the $5d\ ^4[F]_{7/2}$–$6p\ ^4[D]_{5/2}$ transition with an amplified tunable single-mode external cavity laser diode and applied photocounting technique for time-resolved LIF measurements of Xe II velocity in a

stabilized ExB discharge. MacDonald *et al.* [30] derived time-synchronized axial Xe II velocities in the discharge channel and plume of a diverging cusped field thruster from LIF measurements of the $5d[4]_{7/2}$–$6p[3]_{5/2}$ excited state transition centered at 834.724 nm. A tunable CW diode laser was used. Young *et al.* [13] used the same transition to extend the applicability of this time-synchronized sample-hold LIF method for measuring time-varying Xe II velocities to higher frequencies of quasi-coherent natural oscillations in a ExB Hall plasma accelerator. They used a tunable diode laser and beam diagnostics to accurately reconstruct the laser wavelength scan. For the latter, a stationary frequency reference is obtained using the optogalvanic effect with the $6s'[1/2]_1$–$6p'[3/2]_2$ Xe I transition at 834.682 nm in a xenon hollow cathode lamp. This neutral transition was not probed in the Hall plasma accelerator. Diallo *et al.* [31] employed a tunable diode laser to pump the $5d\ ^2[F]_{7/2}$ Xe II metastable level to $6p\ ^2[D]^0_{5/2}$ and performed VDF time-resolved measurements in a CHT using a novel heterodyne method.

On the other hand, less works have been devoted to the LIF study of either neutrals or both neutrals and singly ionized species. Cedolin *et al.* [32] performed LIF in the plume of a laboratory-model xenon Hall thruster based on the Xe I $6s[3/2]^0_2$–$6p[3/2]_2(^3P_2 - {}^1D_2)$ transition at 823.2 nm and Xe II $5d[3]_{7/2}$–$6p[2]^0_{5/2}(^4D_{7/2} - {}^4P_{5/2})$ transition at 605.1 nm. Two lasers were used: a tunable AlGaAs semiconductor diode laser for Xe I and a tunable dye laser pumped by an argon-ion laser for Xe II. Hargus and Cappelli [18] (2001) described the results of LIF velocimetry of both Xe I and Xe II in the plume and interior portions of the acceleration channel of a Hall thruster plasma discharge. They probed the electronic state transitions $6s[3/2]^0_2$–$6p[3/2]_2$ (823.2 nm) and $5d[4]_{7/2}$–$6p[3]_{5/2}$ (834.7 nm) for Xe I and Xe II, respectively. A tunable single-frequency titanium sapphire laser pumped by a Nd:YAG solid-state laser was used. Mazouffre *et al.* [15] studied the xenon atom flow in the cross-field discharge of a Hall thruster through two different electronic transitions, by using an amplified tunable single-mode external cavity laser diode operating in the near-infrared spectral domain. Xe I in the $6s[1/2]^0_2$ level was probed by exciting the $6s[1/2]^0_2$–$6p[3/2]_2$ transition at 834.6822 nm and also Xe I in the $6s[3/2]^0_2$ level was probed by exciting the $6s[3/2]^0_2$–$6p[3/2]_2$ transition at 823.1633 nm. Xe II study was beyond the scope of this specific work. Pawelec *et al.* [33] reported on the experimental determination of the hyperfine splitting of the Xe I lines at 828.01 and 834.68 nm, and the Xe II line at 834.72 nm. A tunable single-mode diode laser was used for Doppler-free spectroscopy. Dancheva *et al.* [20] performed near-exit nonresonant LIF in a Hall effect low-power xenon thruster, and measured axial and radial velocity components exciting the $6s\ ^2[3/2]^0_2$–$6p\ ^2[3/2]_2$ transition at 823.16 nm (Xe I) and the $5d[4]_{7/2}$–$6p[3]^0_{5/2}$ transition at 834.724 nm (Xe II). For this purpose, a diode laser system was built using two standard Fabry–Perot index-guided semiconductor chips, i.e., one for the Xe I transition and one for the Xe II excitation. Crofton *et al.* [14] measured the absolute spatially resolved neutral xenon density in the near-field plume of an operating Hall thruster (SPT-140).

TABLE I
DATA USED IN THIS PAPER (SOURCE: NIST)

	Xe I	Xe II
Wavelength in air (nm)	834.68217	834.724
Wavelength in vacuum (nm)	834.91157	834.953
Zero detuning freq. in vacuum (GHz)	359070.911	359053.094
Speed of light in vacuum (m s^{-1})	299792458	
Planck's constant (eV s)	4.135667662 x10^{-15}	
Boltzman constant (J K^{-1})	1.38064852 x10^{-23}	
Xe molecular weight (g mol^{-1})	131.293	

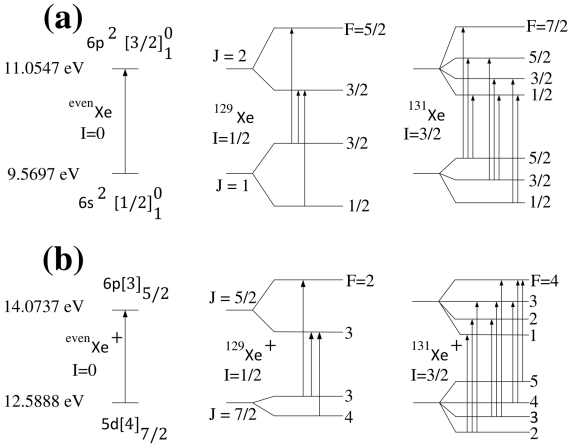

Fig. 1. LIF scheme used for (a) Xe I and (b) Xe II study (energy values are from NIST; diagram not in scale). ISs are not distinguishable on these conceptual energy diagrams, but they are taken into account in this paper (see Fig. 6 and discussion there).

Two-photon (2 × 222.5 nm) laser absorption was used to excite ground state xenon atoms ($5p^6\ ^1$S, $J = 0$) to upper state ($6p'$ [1/2], $J = 0$), which fluoresced at relatively long wavelengths ($6s'$ [1/2], $J = 1$; 788.7 nm) as it transitioned quickly to other levels. An injection-seeded Nd:YAG laser generated 532- and 355-nm pulses. The 532-nm photons were used to pump a dye laser operating on Rhodamine dye at 597.3 nm. The 597- and 355-nm beams were mixed in a BBO crystal to generate 222.5-nm UV pulses. This paper was devoted only to neutrals, excluding ions. Fabris *et al.* [34] presented spatially and temporally resolved LIF measurements of Xe I and Xe II velocity distribution functions in a 400-W Hall thruster during breathing mode. For studying neutral dynamics, they applied a resonant LIF scheme using the Xe I $6s[3/2]^0_2$–$6p[3/2]_2$ transition (823.16 nm) optically pumped by an external cavity diode laser. For measuring ion velocities, the $5d[4]_{7/2}$–$6p[3]_{5/2}$ Xe II transition (834.72 nm) was pumped with a diode laser. The exciting laser beam was generated by a semiconductor-tapered amplifier seeded by a tunable external cavity diode laser through a polarization-maintaining optical fiber.

D. Claims of This Paper

In this paper, the electronic transitions $6s\ ^2[1/2]^0_1$ to $6p\ ^2[3/2]^0_1$ and $5d[4]_{7/2}$ to $6p[3]_{5/2}$ are laser-induced for Xe I (neutral) and Xe II (ion) detection, respectively. The corresponding decay states are $6s[3/2]^0_1$ and $6s[2]_{3/2}$, leading to fluorescence signal at 473.415 and 541.915 nm, respectively. Table I provides related data used here and conceptual diagrams of the transitions are given in Fig. 1.

TABLE II
COMPARISON OF LIF FEATURES FROM INDICATIVE REPORTS

Species Probed	Transition Used	Pumping Wavelength	Setup Employed	(Year) [Reference]
Xe II	$5d\ ^4[F]_{5/2} - 6p\ ^4[D]_{5/2}$	834.7 nm	Continuous wave, single-mode, GaAlAs semiconductor laser.	(1994) [24]
Xe II	It is not mentioned.	834.7 nm	Tunable diode laser.	(2005) [25]
Xe I	It is not mentioned.	834.68 nm (Xe lamp)	Tunable diode laser (the same as for ions).	
Xe II	$5d\ ^2F_{7/2} - 6p\ ^2D^0_{5/2}$ $5d\ ^4D_{7/2} - 6p\ ^4P^0_{5/2}$	834.7 nm 605.1 nm	Tapered-amplifier diode laser. Dye laser (for optogalvanic spectra that provided Doppler broadening function for modeling the 834.7 nm absorption line).	(2005) [26]
Xe II	$5d[4]_{7/2} - 6p[3]^0_{5/2}$	834.7 nm	Diode laser.	(2009) [17]
Xe II	$5d\ ^4F_{5/2} - 6p\ ^4D_{5/2}$	834.7 nm	Tunable diode laser.	(2010) [27]
Xe II	$5d\ ^4D_{7/2} - 6p\ ^4P_{5/2}$	605.278 nm	Continuous wave Ar ion-pumped dye laser.	(2010) [28]
Xe II	$5d\ ^4F_{7/2} - 6p\ ^4D_{5/2}$	834.7 nm	Amplified tunable single-mode external cavity laser diode.	(2013) [29]
Xe II	$5d[4]_{7/2} - 6p[3]_{5/2}$	834.72 nm	Tunable CW diode laser.	(2014) [30]
Xe II	$5d[4]_{7/2} - 6p[3]_{5/2}$	834.724 nm	Tunable diode laser.	(2015) [13]
Xe I	$6s'[1/2]_1 - 6p'[3/2]_2$	834.682 nm (Xe lamp)		
Xe II	$5d\ ^2F_{7/2} - 6p\ ^2D^0_{5/2}$	834.7233 nm	Tunable diode laser.	(2015) [31]
Xe II	$5d[3]_{7/2} - 6p[2]^0_{5/2}$ ($^4D_{7/2} - {}^4P_{5/2}$)	605.1 nm	Tunable dye laser pumped by an argon-ion laser.	(1997) [32]
Xe I	$6s[3/2]^0_2 - 6p[3/2]_2$ ($^3P_2 - {}^1D_2$)	823.2 nm	Tunable AlGaAs semiconductor diode laser.	
Xe II	$5d[4]_{7/2} - 6p[3]_{5/2}$	834.7 nm	Tunable single-frequency titanium sapphire laser pumped by a Nd:YAG solid state laser.	(2001) [18]
Xe I	$6s[3/2]^0_2 - 6p[3/2]_2$	823.2 nm		
Xe I	$6s[1/2]^0_2 - 6p[3/2]_2$ $6s[3/2]^0_2 - 6p[3/2]_2$	834.6822 nm 823.1633 nm	Amplified tunable single-mode external cavity laser diode.	(2011) [15]
Xe II	$5d\ ^4F_{7/2} - 6p\ ^4D_{5/2}$	834.7227 nm	Tunable single-mode diode laser.	(2011) [33]
Xe I	$6s'[1/2]^0_2 - 6s'[3/2]_2$ $6s[3/2]^0_1 - 6p[1/2]_0$	834.6823 nm 828.0116 nm		
Xe II	$5d[4]_{7/2} - 6p[3]^0_{5/2}$	834.724 nm	Diode laser system was built using two standard Fabry-Perot index-guided semiconductor chips, i.e. one for Xe I and one for Xe II excitation.	(2013) [20]
Xe I	$6s\ ^2[3/2]^0_2 - 6p\ ^2[3/2]_2$	823.16 nm		
Xe I	$5p^6\ ^1S;J=0 - 6p'[1/2];J=0$	2x 222.5 nm	Injection-seeded Nd:YAG laser generated 532 nm and 355 nm pulses. The 532 nm photons were used to pump a dye laser operating on Rhodamine dye at 597.3 nm. The 597 nm and 355 nm beams were mixed in a BBO crystal to generate 222.5 nm uv pulses.	(2013) [14]
Xe II	$5d[4]_{7/2} - 6p[3]_{5/2}$	834.72 nm	Semiconductor tapered amplifier seeded by a tunable external cavity diode laser.	(2015) [34]
Xe I	$6s[3/2]^0_2 - 6p[3/2]_2$	823.16 nm	External cavity diode laser.	
Xe II	$\mathbf{5d[4]_{7/2} - 6p[3]_{5/2}}$	**834.72 nm**	**Single tunable diode laser for probing both Xe I and Xe II.**	**This work.**
Xe I	$\mathbf{6s\ ^2[1/2]^0_1 – 6p\ ^2[3/2]^0_1}$	**834.68 nm**		

Table II summarizes the LIF features from the aforementioned representative excellent works in the same order as they are cited in the text. The only report where the present pumping wavelengths are both applied to plasma setups (not in lamps) is the one of reference [33]. But still, reference [33] deals with radio frequency inductively coupled plasma and focuses on the determination of hyperfine structure constants of some lines.

This paper refers to an ambipolar plasma flow in a CHT and examines the Xe I and Xe II line shapes under various operating conditions, i.e., different pressures, gas flow rates, and anode currents. Adjacent wavelength transitions by employing a simple tunable diode laser are pumped. It is thus demonstrated that it is possible to probe both Xe I and Xe II species with a simple LIF system and evaluate the correlation between neutral and ion dynamics. The Hall thruster simulation community is also interested in the behavior across a wide range of operating conditions, using experimental observations to validate and improve existing modeling capability [16]. Making certain assumptions or by properly deconvolving out line-shaped distortions, the LIF profiles can provide valuable information on physical mechanisms through VDFs. This option is presented comprehensively with respect to the present results. The experimental approach is presented in detail in Section II, and the results are given and discussed in Section III. Conclusions and prospective are drawn in Section IV.

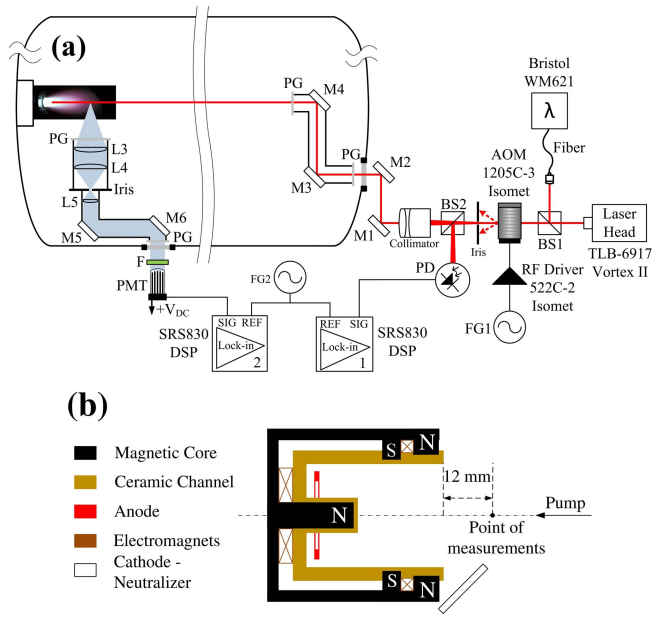

Fig. 2. (a) Block diagram of the LIF setup and its installation in relation to the thruster vacuum chamber. BS: beam splitter; AOM: acousto-optic modulator; PD: photodiode; M: mirror/prism; PG: protective glass; F: filter; PMT: photoelectron multiplier tube; FG: frequency generator. (b) Probed region with respect to the CHT configuration (see [35]–[37] for details).

II. Experimental Setup

The present experiments are performed at the Princeton Plasma Physics Laboratory (PPPL) in a 2.6-cm CHT installed in a vacuum chamber of 0.1-μTorr base pressure. The concept for this thruster and its miniaturized design have been reported extensively elsewhere [35]–[37]. For the purpose of this paper, the thruster is operated without applied magnetic field and discharge individual parameters are mentioned in Section III. In this unusual operating regime, the ions are accelerated from the channel by ambipolar electric field rather than by the $J \times B$ force as for normal Hall thruster operation [38], including CHT operation [1]. Here, the motivation is to explore the feasibility of diagnosing neutrals and ions in a low-power ambipolar plasma source under various conditions for miniaturized plasma propulsion, using LIF diagnostic with a single simple laser head. In the described experiments, the plasma in the CHT channel is produced by a low-pressure gas discharge between the anode and a thermionic hollow cathode. Like in normal Hall thruster operation, the anode serves as a gas distributor. A thermionic hollow cathode is placed outside the thruster channel as described in [39]. During the CHT operation as an ambipolar plasma source, the role of the hollow cathode is to maintain the discharge.

In separate sets of experiments, a comparable operation with a thermionic filament cathode was also tested [40]. However, the limited lifetime of a hot filament cathode (about 2–3 h) makes it generally inconvenient for longer duration thruster experiments [40]; a single LIF scan lasts here typically between 5 and 25 min, depending on the signal-to-noise ratio and the resolution demanded.

The conceptual view of the LIF system built for this paper is depicted in Fig. 2(a), while Fig. 2(b) depicts the region of measurements with respect to the CHT exit plane. The axis of measurements coincides with the thruster axis.

The laser beam is produced by a TLB-6917 Vortex II laser. It is a 60-mW external cavity diode laser based on Littman–Metcalf design. It has single-mode operation with narrow linewidth and precise wavelength tuning. The short-term linewidth is <300 kHz (over a 50-ms time interval), compared with typical line widths for Fabry–Perot diode lasers of 10–500 MHz. The lasing wavelength is controlled by driving a piezoelectric actuator to rotate the end mirror of the laser, using LabVIEW-based interface.

The beam is then split (BS1), and the sampled part is directed into the core of an optical fiber (using an *LC*-1 fiber-optic input coupler). The fiber is connected to a 621-A near-infrared response Bristol wavelength/power meter having continuous calibration due to a built-in stabilized single-frequency He–Ne laser (accuracy ±0.0002 nm at 1000 nm). The rest part of the beam is periodically deflected by an acousto-optic modulator (AOM; PbMoO4, 80 MHz, 1205C-3 Isomet) driven by a digital modulation RF driver (522C-2 Isomet) operating here at 1 kHz (FG). The deflected beam sees an iris, and the resulting chopped beam is sampled (BS2) by a photodiode (PD). This beam chopping is necessary in order to distinguish the fluorescence signal from the spontaneous plasma emission at the wavelengths of interest (see Fig. 2 and next lines for how this distinction is achieved with the lock-in Amplifiers).

The beam pulses pass from a collimator and two mirrors (M1 and M2), and thus enter to the vacuum chamber.

Two dielectric turning prisms (M3 and M4, 750–1100 nm) are housed and aligned in aluminum tubes installed in the vacuum chamber, guiding the beam pulses to the center of the thruster channel coaxially [Fig. 2(b)]. The tube ends are closed by float glass windows (PG) protecting thus the prisms from any deposition due to chamber sputtering from energetic ions. A combination of planoconvex lenses (L3 and L4) and an iris is used to focus on different points on the laser axis due to the adjustable-length tubes between the prisms M5 and M6 (see below for their features), collecting thus the fluorescence signal from the corresponding irradiated plasma elementary volume. The rays of the collected photons are then collimated (L5) on a half-inch surface and transferred outside the vacuum chamber through two dielectric turning prisms (M5 and M6, 400–750 nm). Both prisms are protected similar to M3 and M4 above (PG).

The emission at 473.4 nm (Xe I) and 541.9 nm (Xe II) is extracted from the collected light with a 473/2 nm (Semrock) and a 540/10 nm (ThorLabs) bandpass filter (F), respectively, placed in front of the light detector (PMT; Hamamatsu H10425-01). Both the PMT (lock-in amplifier 2; SRS830 DSP) and PD (lock-in amplifier 1; SRS830 DSP) signals are locked-in to the reference frequency (FG; 1 kHz). Consequently, the fundamental component, due to laser beam chopping, of the LIF and PD signals are singled out. The PD signal monitoring is essential in order to ensure stable phase and amplitude of the laser chopped beam during LIF signal acquisition.

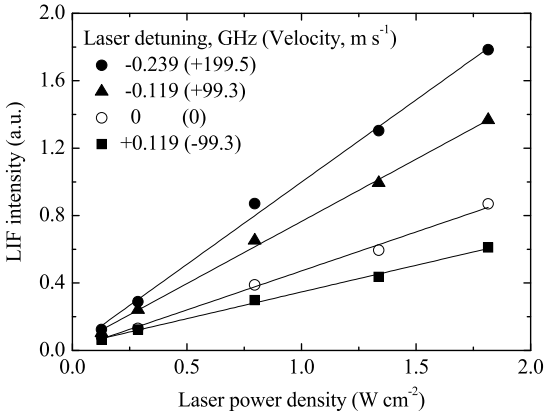

Fig. 3. LIF intensity at 473.415 nm (Xe I) emitted by neutrals excited at three different laser frequencies in the ambipolar plasma, versus the laser power density (laser beam diameter ∼2 mm). In any case, the optical geometry is fixed. Linear fittings to experimental data symbols are shown.

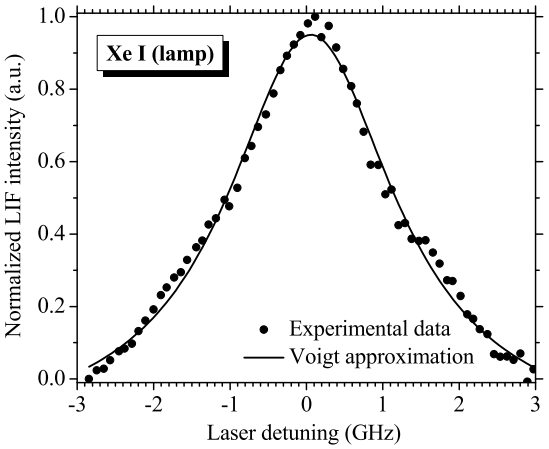

Fig. 4. Indicative LIF normalized data from neutrals in xenon lamp (Newport 6033) approximated with Voigt function.

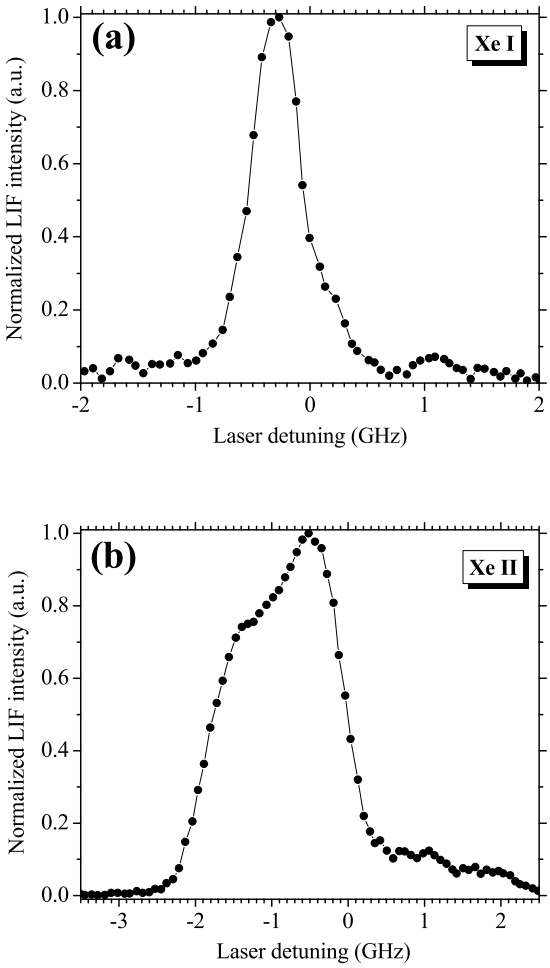

Fig. 5. (a) Xe I and (b) Xe II normalized line shapes. Gas pressure 58 μTorr; anode gas flow rate 3 sccm; cathode gas flow rate 2 sccm; anode current 0.793 A; and anode voltage 67.5 V.

When the laser intensity is sufficiently high to saturate a transition, the fluorescence excitation line shape is broader than the spectral line shape and the fluorescence intensity is less than it would be if it was linear with the laser intensity [18]. In our case, tests on the Xe I and Xe II transitions ensure that such line-shaped distortions are prevented, since a linear relation between the detected fluorescence intensity and the incident laser output power density is established (e.g., see Fig. 3 for the Xe I case).

Finally, a spectral calibration lamp of xenon (Newport 6033) is used in the place of the ambipolar discharge for testing the reliability of the LIF setup and calibrating it in terms of photon frequency. A typical pattern for this stationary absorption is shown in Fig. 4, giving an expected symmetrical distribution around zero since atomic absorbers in the lamp should principally be subjected to thermal random motion. However, the profile deviates from a Gaussian one and a Voigt function gave the best numerical fit, possible due to collisional broadening. The fitting curve peaks at +0.054 GHz and thus laser detuning agrees with NIST data (Table I) by this amount. The Xe II transition is not detectable in this lamp. Similarly, it has also been reported that the glow discharge in the tube used in [17] did not support a sufficient population of excited state ions and the use of this glow discharge tube was only possible for neutral xenon.

III. Results and Discussion

Normalized line shapes of Xe I and Xe II, under typical operating conditions, are given in Fig. 5(a) and (b), respectively. Discrete features are observed on both raw spectra. These features are interpreted below in detail. The main claim of this paper refers to the possibility of parametric study of an ambipolar xenon plasma flow by means of a simple LIF scheme which probes both neutrals and ions under various operating conditions. The viability of the concept is demonstrated in this section by providing the corresponding line shapes. However, in order to further exploit the raw LIF signals, we discuss to what extend these line shapes are potentially distorted due to the mechanisms noted above and finally to what extent they represent VDFs of the probed species.

First of all, due to the absent of external magnetic field, Zeeman splitting may be ignored. Furthermore, the laser

linewidth is typically 300 kHz. Thus, it is about 3–4 orders of magnitude lower than the full-width at half-maximum (FWHM) of the recorded line shapes (∼0.5 GHz for Xe I and ∼1.8 GHz for Xe II, based on Fig. 5) and 2 orders of magnitude lower than the typical resolution applied here (∼65 MHz for Xe I and ∼75 MHz for Xe II, based on Fig. 5). Then, natural broadening for Xe I and Xe II lines is on the order of tens of MHz ([41] and [17], respectively), i.e., about 2 orders of magnitude lower than the FWHM of the present line shapes and marginally close to the applied resolution. It is hence fairly negligible. Regarding the pressure broadening, in plasmas with ions and electrons present in sufficiently high densities (say, at least 1% of the total density) the long-range Coulomb forces are dominant, and one is only concerned with Stark broadening [42]. But still, in a typical Hall thruster, the electric field is several orders of magnitude smaller than what is necessary to make the Stark effect noticeable [43]. Typical plasma density in a conventional Hall thruster is 10^{11}–10^{12} cm^{-3} [36], whereas Stark broadening starts to become noteworthy for densities of orders of magnitude higher [42]. Moreover, the ignorable influence of the above effects is further confirmed here by integrating their impact on a total broadening of the order of 100 MHz and computing synthetic line shapes. Extracted VDFs remain practically unaffected. Hence, the remaining effects of HFS and IS should be the prominent potential distortion sources for the VDFs that correspond to the present registered line shapes.

Indeed, naturally occurring xenon is rich in both isotopes (nine of them are stable) and hyperfine structures. The hyperfine energy levels depend on the total angular momentum $\mathbf{F}$ of the atom: the sum of the total electron angular moment $\mathbf{J}$ and the nuclear-spin angular momentum $\mathbf{I}$, i.e., $\mathbf{F} = \mathbf{J} + \mathbf{I}$. The magnetic dipole and electric quadrapole moments of the nucleus are characterized by the hyperfine structure constants [44], the knowledge of which is necessary for calculating the hyperfine energy shifts from the position of the energy for the unshifted level with angular momentum $\mathbf{J}$ [18]. The nine isotopes of xenon each have a slight difference in their electron transition energies due to their differences in mass [14], [18]. Furthermore, five of them have high natural abundances between 8.9% and 26.4% [14]. Each of these isotopes causes a shift of the energy levels (isotopic splitting) involving a transition of a few tens of MHz [28]. Of the nine isotopes of xenon, seven have an even atomic mass. Thus, they have a nuclear spin $\mathbf{I} = 0$ and do not contribute to the nuclear-spin splitting. The remaining two (^{129}Xe and ^{131}Xe) are odd mass isotopes and are further spin split due to nuclear magnetic dipole and electric quadrapole moments [14], [18]. Both ISs in the center of gravity of the transition frequency and hyperfine splitting for some of the isotopes contribute to line broadening; however, the hyperfine contribution typically dominates when present [14]. This nuclear-spin splitting is considerably larger (1 to 2 orders of magnitude [45]) than the isotopic splitting and is responsible for most of the characteristics of the line shapes [28]. Typically, xenon HFSs have frequency shifts of 10–1000 MHz, which are comparable with the FWHM of the average VDFs in a Hall thruster and can hence add large distortions to the raw data [17].

On the other hand, the LIF signal deconvolution for obtaining reliable VDFs is not straightforward due to the need of knowledge of the hyperfine structure shift energies and relative intensities. The Xe II transition at 834.7 nm has a total of nineteen isotopic and spin split components, but there are data only on the nuclear splitting constants of the upper state and no information is available on the transition-dependent isotope shifts [18]. The lower state hyperfine structure constants are unknown [17], and the lack of published hyperfine structure constants for this transition has been mentioned [21], although accurate estimation of some of them has been realized [33]. Instead, the hyperfine structure has been shown to be around 500 MHz wide in photon frequency space [17] and if the width of the LIF signal is much larger than the spread of the lines of the transition, then the LIF signal can be taken directly as the projected velocity distribution function [46]. On the top of that, previous work with the Xe II transition at 834.7 nm in Hall thruster discharges suggests that deconvolution from the LIF line shapes may not be necessary to resolve the ion VDF [47]. In any case, the most probable velocity is recovered simply from the location of the Doppler-shifted LIF signal peak [13].

Regarding the Xe I transition at 834.682 nm, the HPS constants are well established [45], [48] and since the Xe I LIF signals are narrower than the Xe II ones (Fig. 5), hyperfine splitting becomes more critical for neutral VDF determination.

In this paper, a numerical code is developed in a multiparadigm numerical computing environment to take into account VDF distortions due to HPS and IS. The resultant centers and relative peak intensities of the line-shaped components are shown in Fig. 6. For Xe I, the method explained in [45] is applied. Energy levels are from NIST atomic spectra database, while HPS constants, isotopic abundances, and shifts are from [45]. For the Xe II species, the same method as in [26] and [45] is used. Energy levels are from NIST, HPS constants from [33], and isotopic abundances from [45]. In the absence of IS values for the transition $5d[4]_{7/2}$–$6p[3]_{5/2}$, the use of published data for the similar transition $5d\ ^4D_{7/2}$–$6p\ ^4P_{5/2}$ (605.1 nm) has been suggested [24] and values from [49] are here adopted. It should, however, be emphasized that important discrepancies between available data are appeared even for this "known" transition (e.g., compare [26] and [49]).

Then, since raw LIF signals correspond to the convolution of HPS/IS components with actual VDFs, a VDF could be extracted through deconvolution process. However, this treatment does not provide reliable results here, due to the amplification of the noise-to-signal ratio during numerical deconvolution. In its place, a comparable process for extracting VDFs is followed. After several numerical tests, it was found that it was not possible to fit the synthetic like shapes to the LIF signals along the entire detuning range with the use of a single Gaussian. The fit was poor and residual was reaching high values. Instead, velocity distributions appear to fairly approach bi-Gaussian functions which are numerically convolved with the components of Fig. 6 to provide synthetic line shapes. Three free parameters (i.e., FWHM, peak abscissa,

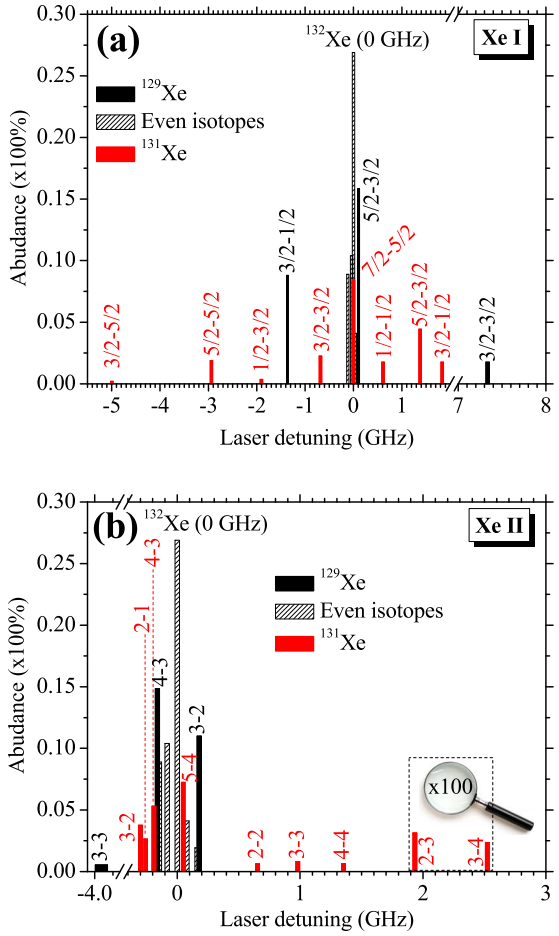

Fig. 6. Centers and relative peak intensities of the line-shaped components, as calculated by the numerical code developed for this paper (a) Xe I and (b) Xe II. The transitions are given with respect to the energy diagram of Fig. 1 and the even isotope ^{132}Xe is arbitrary used as reference in photon frequency space due to its higher abundance. See text for the bibliographic sources of the hyperfine structure constants and IS values used.

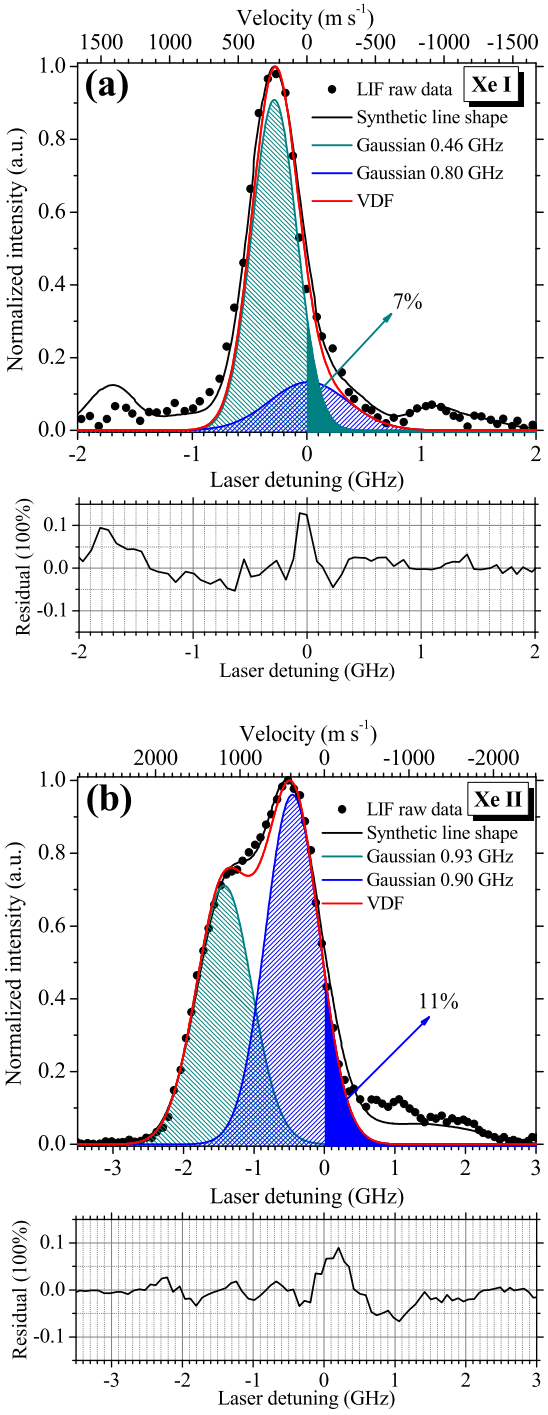

Fig. 7. (a) Xe I LIF raw signal of Fig. 5(a) compared with the synthetic line shape and the corresponding VDF. (b) Xe II LIF raw signal of Fig. 5(b) compared with the synthetic line shape and the corresponding VDF. The subgraphs provide a quality factor of the VDF extraction process, since it equals the residual between the synthetic and measured line shape.

and area under curve) for each Gaussian function are allowed varying independently and the optimum set of them is computed by means of trial-and-error method.

Fig. 7(a) compares the synthetic line shape with the raw LIF data of Fig. 5(a) and the corresponding Xe I VDF. Two neutral populations are present under the bi-Gaussian assumption. A "cold" one (0.46 GHz/420 K) which dominates and a "hot" one (0.8 GHz/1270 K) of lower density (ratio 4:1, respectively). The former has an axial velocity component $+250$ m·s^{-1}, and the latter has practically zeroed axial velocity component (essentially thermal).

The Xe II LIF signal of Fig. 5(b) is similarly treated, and the results are given in Fig. 7(b). Evidently, Xe II VDF is bimodal. The existence of such VDFs has been previously established in helicon plasmas [28] and Hall effect thrusters [34], [46], whereas it is demonstrated here for an ambipolar discharge. The "slow" ion population has most probable axial velocity 370 m $\cdot$ s^{-1} and the "fast" one peaks at $+1200$ m $\cdot$ s^{-1}. Their density ratio is 1.3:1, respectively.

The Xe I "cold" population corresponds to atoms from the jet. The "hot" one may comprise atoms that are thermalized with the channel walls and anode (when we turn thruster off, we do see glowing anode) or gain energy through charge-exchange collisions with energetic ions. Although with the data of this paper, we can make only assumptions on the origin of this "hot" minor population, we have seen that it is not affected significantly by the background pressure, cathode gas flow or anode current variation. It is, however, quite

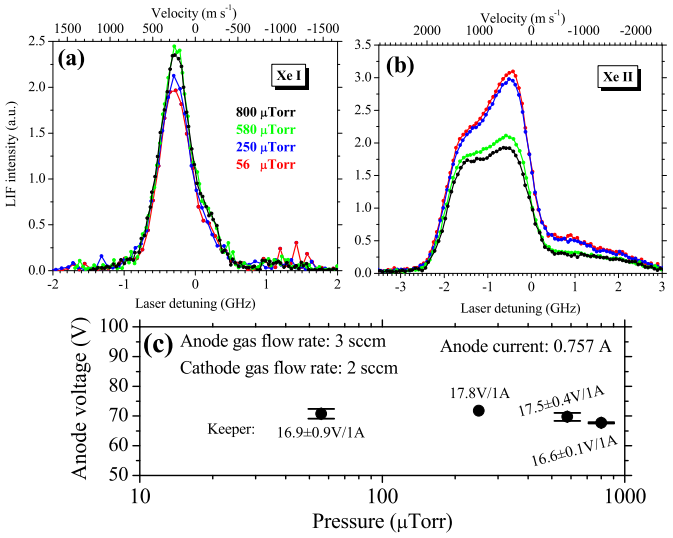

Fig. 8. (a) Xe I and (b) Xe II line shapes with the xenon pressure as a variable parameter. (c) Corresponding CHT conditions during LIF scans.

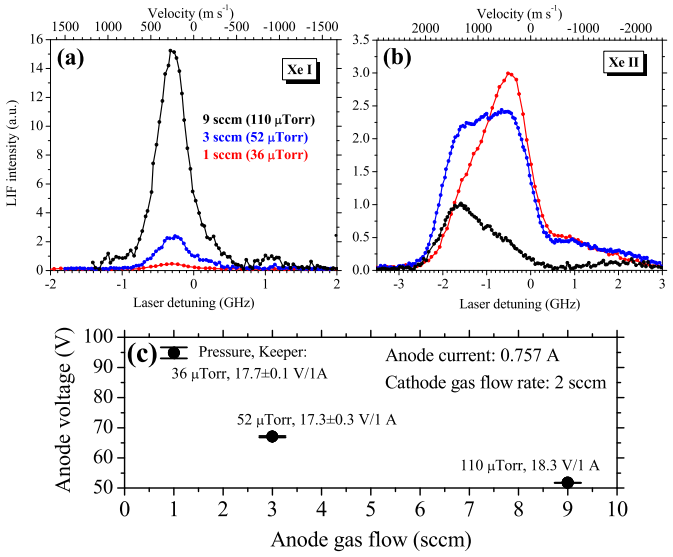

Fig. 9. (a) Xe I and (b) Xe II line shapes with the anode gas flow rate as a variable parameter. (c) Corresponding CHT conditions during LIF scans.

dependent on the anode gas flow (results below). Furthermore, a part of the "cold" population has negative axial velocity component [7% in Fig. 7(a)] which should originate in charge-exchange collisions [15]. With typical values of the mean free path of Xe I to be around 0.3 m at 300 K, 0.5 m at 500 K, and 1 m at 1000 K, for a background pressure of 100 μTorr [50], the anticipated back flux should be very low, whereas in our experiments, the amount of negatively propagating neutrals is quite high. Thus, simple backscattering process is excluded as main reason for negative velocities of neutrals. This is further confirmed by Fig. 8(a), since this negative-velocity part is nearly insensitive to pressure variation in a wide range, between 56 and 800 μTorr.

In the case of Xe II, the "slow" population also exhibits a negative-velocity part, i.e., 11% in Fig. 7(b). This portion is comparable with the negative-velocity part of the "cold" neutrals. Other works have indeed confirmed that slow ions produced near the centerline in the vicinity of the exit plane are accelerated toward the source body with a negative-velocity [51]. The "fast" ions have only positive velocities. Many experimental tests were performed to insure that any negative component is not an artifact of our measurements. This component is due to ions propagating along the laser beam toward the anode of the ambipolar discharge. Anode floats below the plasma potential and so ions may be accelerated to the anode. In the concept of this paper, we cannot comment further on this topic and it remains a prospective, which requires spatially resolved measurements.

Hereafter, acquired line shapes of Xe I and Xe II species are exposed and commented, proving the sensitivity of the proposed LIF scheme to operating parameter variation for capturing both ion and neutral dynamics. All signals preserve the above discussed main structural features, whereas variations on the intensity, most probable velocity, and broadening are noticed. Thus, these distinguishable features are outlined from the LIF raw data and VDFs are extracted wherever

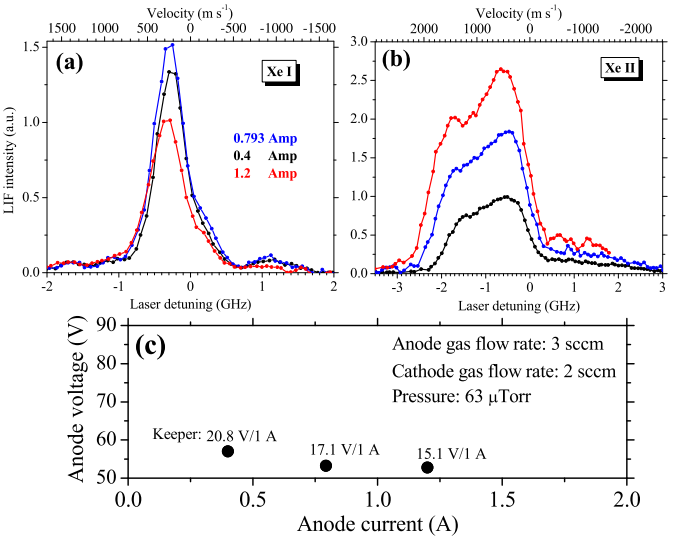

Fig. 10. (a) Xe I and (b) Xe II line shapes with the anode current as a variable parameter. (c) Corresponding CHT conditions during LIF scans.

further analysis is needed. Figs. 8–10 are concerned with the Xe I and Xe II line-shaped modification as a function of the background pressure, anode gas flow rate and anode current, respectively.

Neutrals are highly affected in density when the gas pressure increases by introducing gas through the anode [Fig. 9(a)]. Pressure variation over the same range by introducing gas from chamber top flange, affects slightly the neutral density [Fig. 8(a)]. At the same time, the "hot" population does not change proportionally and it is more affected by the anode gas flow variation [see Fig. 9(a) versus Fig. 8(a)]. Independently of the pressure and the anode gas flow, within the present operating conditions, the neutral most probable velocity varies in a narrow range (260 ± 30 m $\cdot$ s^{-1}).

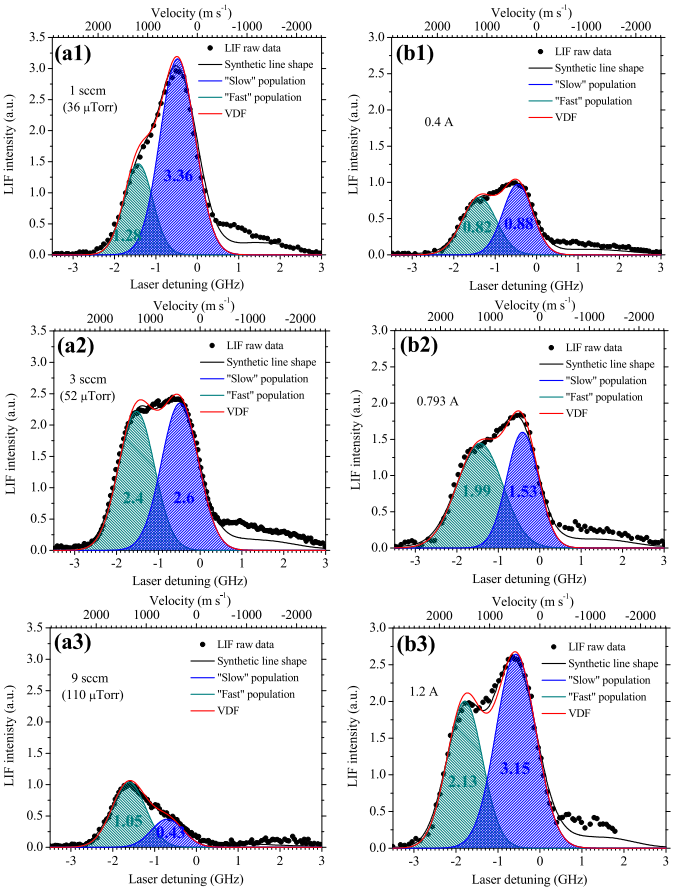

Fig. 11. Treatment of the line shapes of Figs. 9(a1)–(a3) and 10(b1)–(b3) for comparing the "slow" and "fast" population evolution during anode gas flow (a1)–(a3) and anode current (b1)–(b3) variation.

Gas pressure increase, especially through anode gas flow, has a dramatic influence on the ion LIF signal, on both "slow" and "fast" populations. In Fig. 8(b), ion density decreases with pressure, but the portion between the two populations does not change significantly. In contrast, anode gas flow variation completely modifies the two ionic populations, with the "fast" one to dominate the "slow" as the gas flow rate increases. During flow rate variation, pressure changes too, but the pressure values are comparable to that of Fig. 8. Thus, the anode gas flow role is quite isolated. Analytically, in Fig. 11(a1)–(a3), the corresponding LIF signals are treated to extract VDFs and the relative density of both populations, integrated over the photon frequency domain, is given. The ratio "slow" to "fast" changes from 2.6 to 1.08 and last 0.41 as the anode gas flow rate varies from 1 to 3 and 9 sccm, respectively.

The last parameter being varied here is the anode current, by simply changing the current limit of the power supply. Interestingly, anode current affects the "cold" (mainly) neutral density and at the value of 1.2-A neutral depletion at the point of measurements seems to take place possibly due to ion formation increase. Fig. 10(b) presents this increase of the ion LIF signal, while Fig. 11(b1)–(b3) distinguishes the evolution of both ionic populations versus the anode current. Both population density increases. However, under the assumption of bi-Gaussian VDFs, the ratio "slow"-to-"fast" population begins with a value of 1.07, it passes from a minimum of 0.77 at 0.793 A and it gets eventually the value 1.48. Simultaneously, Xe I "cold" population relative density passes from a maximum at 0.793 A, as Fig. 10(a) depicts. Once could propose that "slow" ions dominate at the expense of "cold" neutrals and vice versa.

IV. Conclusion

A single tunable diode laser was employed for pumping the xenon transitions $6s\ ^2[1/2]^0_1$–$6p\ ^2[3/2]^0_1$ and $5d[4]_{7/2}$–$6p[3]_{5/2}$ in an ambipolar plasma flow, by means of laser-induced nonresonant fluorescence. The ambipolar plasma source was a CHT operating without supplying the coils of the magnetic field, in the concept of simplified designs for low-power thrusters. The LIF scheme was tested, and it was shown that the fluorescence signal from the relaxation of both transitions was readily detectable with adequate resolution. Line shapes of neutrals and single-ionized species were recorded under various operating conditions. Velocity distribution functions were extracted from the experimental line shapes. Bi-Gaussian distribution assumption, both for neutrals and ions, gave acceptable agreement between experimentally determined and synthetic line shapes. Neutral and ion velocity distribution functions were found to be affected by the anode gas flow and current, and less by the background pressure. The bulk neutrals showed temperature around 400 K and axial velocity about 250 $\mathrm{m \cdot s^{-1}}$. Ions were accelerated up to about 1500 $\mathrm{m \cdot s^{-1}}$. Correlations between neutrals and ions during the variation of anode-related parameters, demonstrated the need for studying both neutral and charged xenon species for probing discharge dynamics. The present initial tests of our LIF scheme and the development of the numerical code for taking into account hyperfine structure and IS components will allow future targeted studies. For instance, spatially resolved measurements will potentially allow the determination of the origin of each population, including any negative-velocity component.

Acknowledgment

The authors would like to thank S. Keller for fruitful discussions and A. Merzhevsky for the technical support.

References

[1] K. D. Diamant, J. E. Pollard, Y. Raitses, and N. J. Fisch, "Ionization, plume properties, and performance of cylindrical Hall thrusters," *IEEE Trans. Plasma Sci.*, vol. 38, no. 4, pp. 1052–1057, Apr. 2010.

[2] C. Charles, R. W. Boswell, and M. A. Lieberman, "Xenon ion beam characterization in a helicon double layer thruster," *Appl. Phys. Lett.*, vol. 89, no. 26, p. 261503, 2006.

[3] Y. Raitses, A. Smirnov, and N. J. Fisch, "Effects of enhanced cathode electron emission on Hall thruster operation," *Phys. Plasmas*, vol. 16, no. 5, p. 057106, 2009.

[4] A. W. Smith and M. A. Cappelli, "On the role of fluctuations, cathode placement, and collisions on the transport of electrons in the near-field of Hall thrusters," *Phys. Plasmas*, vol. 17, no. 9, p. 093501, 2010.

[5] A. J. Perry and R. W. Boswell, "Fast anisotropic etching of silicon in an inductively coupled plasma reactor," *Appl. Phys. Lett.*, vol. 55, no. 2, pp. 148–150, 1989.

[6] C. Charles, "Ion energy distribution functions in a multipole confined argon plasma diffusing from a 13.56-MHz helicon source," *J. Vac. Sci. Technol. A, Vac. Surf. Films*, vol. 11, no. 1, pp. 157–163, 1993.

[7] A. Fruchtman, "Ambipolar and nonambipolar cross-field diffusions," *Plasma Sources Sci. Technol.*, vol. 18, no. 2, p. 025033, 2009.

[8] B. W. Longmier *et al.*, "Ambipolar ion acceleration in an expanding magnetic nozzle," *Plasma Sources Sci. Technol.*, vol. 20, no. 1, p. 015007, 2011.

[9] C. Rebont, N. Claire, T. Pierre, and F. Doveil, "Ion velocity distribution function investigated inside an unstable magnetized plasma exhibiting a rotating nonlinear structure," *Phys. Rev. Lett.*, vol. 106, p. 225006, Jun. 2011.

[10] B. Beal, A. Gallimore, and W. A. Hargus, Jr., "The effects of clustering multiple Hall thrusters on plasma plume properties," in *Proc. 39th AIAA/ASME/SAE/ASEE Joint Propuls. Conf. Exhibit*, 2003, p. 5155, Paper AIAA 2003-5155.

[11] Y. Raitses, A. Smirnov, and N. J. Fisch, "Enhanced performance of cylindrical Hall thrusters," *Appl. Phys. Lett.*, vol. 90, no. 22, p. 221502, 2007.

[12] C. Charles and R. W. Boswell, "Laboratory evidence of a supersonic ion beam generated by a current-free 'helicon' double-layer," *Phy. Plasmas*, vol. 11, no. 4, pp. 1706–1714, 2004.

[13] C. V. Young, A. L. Fabris, and M. A. Cappelli, "Ion dynamics in an $E \times B$ Hall plasma accelerator," *Appl. Phys. Lett.*, vol. 106, no. 4, p. 044102, 2015.

[14] M. W. Crofton, A. G. H. Schouten, J. A. Young, E. J. Beiting, and K. D. Diamant, "Neutral xenon density in the SPT-140 near-field plume," in *Proc. 33st Int. Electr. Propuls. Conf.*, 2013, pp. 1–41, Paper IEPC-2013-399.

[15] S. Mazouffre, G. Bourgeois, L. Garrigues, and E. Pawelec, "A comprehensive study on the atom flow in the cross-field discharge of a Hall thruster," *J. Phys. D: Appl. Phys.*, vol. 44, no. 10, p. 105203, 2011.

[16] B. Reid and A. Gallimore, "Langmuir probe measurements in the discharge channel of a 6-kW Hall thruster," in *Proc. 44th AIAA/ASME/SAE/ASEE Joint Propuls. Conf. Exhibit*, 2008, p. 4920, Paper AIAA 2008-4920.

[17] W. Huang, T. B. Smith, and A. D. Gallimore, "Obtaining velocity distribution using a xenon ion line with unknown hyperfine constants," in *Proc. 40th AIAA Plasmadynamics Lasers Conf.*, 2009, p. 4226, Paper AIAA 2009-4226.

[18] W. A. Hargus, Jr., and M. A. Cappelli, "Laser-induced fluorescence measurements of velocity within a Hall discharge," *Appl. Phys. B, Lasers Opt.*, vol. 72, no. 8, pp. 961–969, 2001.

[19] W. Demtröder, *Laser Spectroscopy: Basic Concepts and Instrumentation*. New York, NY, USA: Springer-Verlag, 1996.

[20] Y. Dancheva, V. Biancalana, D. Pagano, and F. Scortecci, "Measurement of XeI and XeII velocity in the near exit plane of a low-power Hall effect thruster by light induced fluorescence spectroscopy," *Rev. Sci. Instrum.*, vol. 84, no. 6, p. 065113, 2013.

[21] W. Huang, A. Gallimore, and T. Smith, "Two-axis laser-induced fluorescence of singly-charged xenon inside a 6-kW Hall thruster," in *Proc. 49th AIAA Aerosp. Sci. Meeting Including New Horizons Aerosp. Expo.*, 2011, p. 1015, Paper AIAA 2011-1015.

[22] S. Mazouffre, "Laser-induced fluorescence diagnostics of the cross-field discharge of Hall thrusters," *Plasma Sources Sci. Technol.*, vol. 22, no. 1, p. 013001, 2013.

[23] S. Mazouffre, "Laser-induced fluorescence spectroscopy applied to electric thrusters," in *Electric Propulsion Systems: From Recent Research Developments to Industrial Space Applications—STO-AVT-263*. New York, NY, USA: NATO-STO, 2016, pp. 10-1–10-28.

[24] D. H. Manzella, "Stationary plasma thruster ion velocity distribution," NYMA, Inc., Brook Park, OH, USA, NASA Contractor Rep. 195379, 1994.

[25] N. Gascon, M. Cappelli, and W. A. Hargus, Jr., "Ion velocity measurements in a linear Hall thruster," in *Proc. 41st AIAA/ASME/SAE/ASEE Joint Propuls. Conf. Exhibit*, 2005, p. 4401, Paper AIAA 2005-4401.

[26] T. Smith, B. Ngom, J. Linnell, and A. Gallimore, "Diode laser-induced fluorescence of xenon ion velocity distributions," in *Proc. 41st AIAA/ASME/SAE/ASEE Joint Propuls. Conf. Exhibit*, 2005, p. 4406, Paper AIAA 2005-4406.

[27] R. Spektor, K. D. Diamant, E. J. Beiting, Y. Raitses, and N. J. Fisch, "Laser induced fluorescence measurements of the cylindrical Hall thruster plume," *Phys. Plasmas*, vol. 17, no. 9, p. 093502, 2010.

[28] I. A. Biloiu and E. E. Scime, "Ion acceleration in Ar–Xe and Ar–He plasmas. II. Ion velocity distribution functions," *Phy. Plasmas*, vol. 17, no. 11, p. 113509, 2010.

[29] J. Vaudolon, L. Balika, and S. Mazouffre, "Photon counting technique applied to time-resolved laser-induced fluorescence measurements on a stabilized discharge," *Rev. Sci. Instrum.*, vol. 84, no. 7, p. 073512, 2013.

[30] N. A. MacDonald, M. A. Cappelli, and W. A. Hargus, Jr., "Time-synchronized continuous wave laser-induced fluorescence axial velocity measurements in a diverging cusped field thruster," *J. Phys. D: Appl. Phys.*, vol. 47, no. 11, p. 115204, 2014.

[31] A. Diallo, S. Keller, Y. Shi, Y. Raitses, and S. Mazouffre, "Time-resolved ion velocity distribution in a cylindrical Hall thruster: Heterodyne-based experiment and modeling," *Rev. Sci. Instrum.*, vol. 86, no. 3, p. 033506, 2015.

[32] R. J. Cedolin, W. A. Hargus, Jr., P. V. Storm, R. K. Hanson, and M. A. Cappelli, "Laser-induced fluorescence study of a xenon Hall thruster," *Appl. Phys. B, Lasers Opt.*, vol. 65, pp. 459–469, Oct. 1997.

[33] E. Pawelec, S. Mazouffre, and N. Sadeghi, "Hyperfine structure of some near-infrared Xe I and Xe II lines," *Spectrochim. Acta B, At. Spectrosc.*, vol. 66, no. 6, pp. 470–475, 2011.

[34] A. L. Fabris, C. V. Young, and M. A. Cappelli, "Time-resolved laser-induced fluorescence measurement of ion and neutral dynamics in a Hall thruster during ionization oscillations," *J. Appl. Phys.*, vol. 118, no. 23, p. 233301, 2015.

[35] Y. Raitses and N. J. Fisch, "Parametric investigations of a nonconventional Hall thruster," *Phy. Plasmas*, vol. 8, no. 5, pp. 2579–2586, 2001.

[36] A. Smirnov, Y. Raitses, and N. J. Fisch, "Parametric investigation of miniaturized cylindrical and annular Hall thrusters," *J. Appl. Phys.*, vol. 92, no. 10, pp. 5673–5679, 2002.

[37] A. N. Smirnov, Y. Raitses, and N. J. Fisch, "Electron cross-field transport in a miniaturized cylindrical Hall thruster," *IEEE Trans. Plasma Sci.*, vol. 34, no. 2, pp. 132–141, Apr. 2006.

[38] A. I. Morozov, "The conceptual development of stationary plasma thrusters," *Plasma Phys. Rep.*, vol. 29, no. 3, pp. 235–250, 2003.

[39] A. Smirnov, Y. Raitses, and N. J. Fisch, "Experimental and theoretical studies of cylindrical Hall thrusters," *Phy. Plasmas*, vol. 14, no. 5, p. 057106, 2007.

[40] E. M. Granstedt, Y. Raitses, and N. J. Fisch, "Cathode effects in cylindrical Hall thrusters," *J. Appl. Phys.*, vol. 104, no. 10, p. 103302, 2008.

[41] R. J. Cedolin, R. K. Hanson, and M. A. Cappelli, "Laser-induced fluorescence measurements of resonance broadening in xenon," *Phys. Rev. A, Gen. Phys.*, vol. 54, pp. 335–342, Jul. 1996.

[42] R. H. Huddlestone and S. L. Leonard, *Plasma Diagnostic Techniques*. New York, NY, USA: Academic, 1965.

[43] H. W. Harkness and J. F. Heard, "The stark effect for xenon," *Proc. Roy. Soc. A, Math., Phys. Eng. Sci.*, vol. 139, no. 838, pp. 416–435, 1933.

[44] R. D. Cowan, *The Theory of Atomic Structure and Spectra*. Berkley, CA, USA: Univ. California Press, 1981.

[45] T. B. Smith, W. Huang, B. B. Ngom, and A. D. Gallimore, "Optogalvanic and laser-induced fluorescence spectroscopy of the Zeeman effect in xenon," in *Proc. 30th Int. Electr. Propuls. Conf.*, 2007, pp. 1–13, Paper IEPC-2007-229.

[46] P.-Q. Elias, J. Jarrige, E. Cucchetti, D. Packan, and A. Built, "Full ion velocity distribution function measurement in an electric thruster, using LIF-based tomographic reconstruction," in *Proc. 34th Int. Electr. Propuls. Conf.*, 2015, pp. 1–18, Paper IEPC-2015-235.

[47] D. Gawron, S. Mazouffre, N. Sadeghi, and A. Héron, "Influence of magnetic field and discharge voltage on the acceleration layer features in a Hall effect thruster," *Plasma Sources Sci. Technol.*, vol. 17, no. 2, p. 025001, 2008.

[48] W. Huang and A. D. Gallimore, "Laser-induced fluorescence study of neutral xenon flow evolution inside a 6-kW Hall thruster," in *Proc. 31st Int. Electr. Propuls. Conf.*, 2009, pp. 9–87, Paper IEPC-2009-087.

[49] E. Alvarez *et al.*, "Isotope shift and hyperfine structure measurements in Xe II in a laser-ion beam experiment," *Phys. Scripta*, vol. 20, no. 2, pp. 141–144, 1979.

[50] E. Nasser, *Fundamentals of Gaseous Ionization and Plasma Electronics*. New York, NY, USA: Wiley, 1971.

[51] A. Lejeune, G. Bourgeois, and S. Mazouffre, "Kr II and Xe II axial velocity distribution functions in a cross-field ion source," *Phys. Plasmas*, vol. 19, no. 7, p. 073501, 2012.

Panagiotis Svarnas (SM'13) received the M.Sc. Diploma from the Electrical and Computer Engineering Department, University of Patras, Rion-Patras, Greece, and the Ph.D. Diploma from the same Department and the Physics Department, UPPA, Pau, France.

He was a Research Associate (Post-Doc) with the Ecole Polytechnique, Palaiseau, France, the "Laboratoire de Photonique et des Nanostructures," CNRS-Alcatel, Marcoussis, France, and the Electrical Engineering and Electronics Department, University of Liverpool, Liverpool, U.K.. In 2015, he realized his sabbatical leave to the Princeton Plasma Physics Laboratory, Princeton, NJ, USA. He is currently a tenured Associate Professor with the Electrical and Computer Engineering Department, University of Patras. He has authored and co-authored more than 60 journal articles on plasma physics and applications.

Ivan Romadanov had an internship at the Princeton Plasma Physics Laboratory, Princeton, NJ, USA, where he participated in laser-induced fluorescence diagnostic development for Hall thruster. He is currently a Ph.D. Student with the University of Saskatchewan, Saskatoon, SK, Canada. His current research interests include theoretical and experimental studies of ExB discharges, and their applications for space propulsion.

Ahmed Diallo is currently a Research Physicist with the Princeton Plasma Physics Laboratory, Princeton, NJ, USA, where he is the Leader of the Pedestal Structure and Control Topical Science Group of the National Spherical Torus Experiment-Upgrade. He is developing a fast burst laser system to investigate the dynamics of the edge of fusion devices as well as to control it. He collaborates on many national and international tokamaks. He has more than 15 years of experience in laser-aided plasma diagnostics (e.g., laser-induced fluorescence, Thomson scattering), and he has expertise in polarization spectroscopy. He authored and co-authored more than 100 peer-reviewed papers and has given more than 10 talks at national and international scientific meetings.

Mr. Diallo is a recipient of the DOE Early Career award.

Yevgeny Raitses initiated nanosynthesis research at Princeton Plasma Physics Laboratory (PPPL), Princeton, NJ, USA. He is currently a Principal Research Physicist with the PPPL. He is an Expert in experimental plasma physics. He is the Head of the Laboratory for Plasma Nanosynthesis (LPN-PPPL) with specific responsibility for experimental activities at LPN-PPPL, including plasma and synthesis experiments. He is also directing PPPL research program on plasma thrusters. He has authored over 100 publications on physics of plasma thrusters, plasma–surface interactions, nanosynthesis plasmas, cross-field discharges, and plasma diagnostics.